

Quantum spin liquid and cluster Mott insulator phases in the Mo_3O_8 magnets

S. A. Nikolaev,^{1,2,*} I. V. Solovyev,^{2,3} and S. V. Streltsov^{4,3}

¹*Institute of Innovative Research, Tokyo Institute of Technology,
4259 Nagatsuta, Midori, Yokohama 226-8503, Japan*

²*International Center for Materials Nanoarchitectonics,
National Institute for Materials Science, 1-1 Namiki, Tsukuba, Ibaraki 305-0044, Japan*

³*Department of Theoretical Physics and Applied Mathematics,
Ural Federal University, Mira St. 19, 620002 Yekaterinburg, Russia*

⁴*Institute of Metal Physics, S. Kovalevskoy Street 18, 620108 Yekaterinburg, Russia*

(Dated: January 22, 2020)

We unveil the microscopic origin of largely debated magnetism in the Mo_3O_8 cluster systems. Upon considering an extended Hubbard model at $1/6$ filling on the anisotropic kagomé lattice formed by the Mo atoms, we argue that its ground state is determined by the competition between kinetic energy and intersite Coulomb interactions, which is controlled by the trimerisation of the kagomé lattice into the Mo_3O_{13} clusters. Based on first-principles calculations, we show that the strong interaction limit is realised in $\text{LiZn}_2\text{Mo}_3\text{O}_8$ revealing a plaquette charge order with unpaired spins at the resonating hexagons, whose origin is solely related to the opposite signs of intracluster and intercluster hoppings, in contrast to all previous scenarios. On the other hand, both $\text{Li}_2\text{InMo}_3\text{O}_8$ and $\text{Li}_2\text{ScMo}_3\text{O}_8$ are demonstrated to fall into the weak interaction limit where the electrons are well localised at the Mo_3O_{13} clusters. While the former is found to exhibit long-range antiferromagnetic order, the latter is more likely to reveal short-range order with quantum spin liquid-like excitations. Our results not only reproduce most of the experimentally observed features of these unique materials, but will also help to describe various properties in other quantum cluster magnets.

Introduction. Geometrically frustrated quantum systems lie at the core of research activity revolving around a putative quantum spin liquid (QSL) state that displays long-range quantum entanglement, charge fractionalisation, and emergent gauge structures [1–4]. Of particular importance are spin models on the triangular and kagomé lattices featuring various types of QSL [5–9], whose material realisation has been an ongoing endeavour in condensed matter physics with only a few reasonable candidates proposed so far [10–15].

During the past few years, the Mo_3O_{13} cluster magnets have attracted a great deal of both experimental and theoretical attention as a new candidate to host QSL. In these compounds, the Mo atoms arranged in anisotropic kagomé layers are trimerised, and the $[\text{Mo}_3\text{O}_{13}]^{15-}$ clusters form a triangular lattice, as shown in Fig. 1a [16, 17]. As sketched in Fig. 1b, six out of seven valence electrons in the Mo_3O_{13} cluster are responsible for a strong intracluster metal-metal bonding, and the seventh electron remains unpaired occupying a totally symmetric molecular a_1 state.

$\text{LiZn}_2\text{Mo}_3\text{O}_8$ was first reported to exhibit a QSL behaviour [18–20]. The magnetic susceptibility of $\text{LiZn}_2\text{Mo}_3\text{O}_8$ has been experimentally shown to follow a Curie-Weiss law with low- and high-temperature regimes transitioning at 96 K, whose Curie constants are related as $C_L \approx C_H/3$ and where the disappearance of $2/3$ of paramagnetic spins was attributed to valence bond condensation on the triangular lattice of the Mo_3O_{13} clusters. In a first attempt to explain these unusual features, the authors of Ref. [21] suggested the formation of an emergent honeycomb lattice due to opposite rota-

tions of the Mo_3O_{13} clusters effectively decoupling the central cluster with an orphan paramagnetic spin. Another scenario was outlined in Ref. [22], where a plaquette charge order (PCO) existing in a Mott insulator on the anisotropic kagomé lattice at $1/6$ filling was conjectured to host a $U(1)$ quantum spin liquid state with the spinon

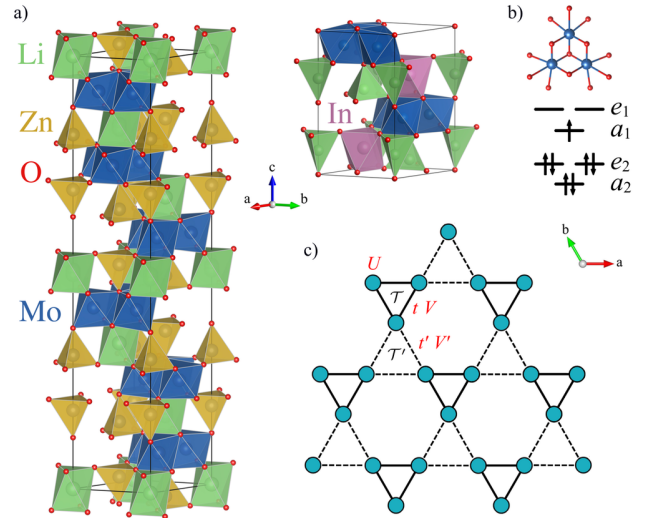


FIG. 1. a) Crystal structures of $\text{LiZn}_2\text{Mo}_3\text{O}_8$ and $\text{Li}_2\text{InMo}_3\text{O}_8$, visualised with VESTA [26]. $\text{Li}_2\text{ScMo}_3\text{O}_8$ is isostructural to $\text{Li}_2\text{InMo}_3\text{O}_8$; b) Molecular levels of the Mo_3O_{13} cluster filled with seven electrons; c) Schematics of the extended Hubbard model on the anisotropic kagomé lattice formed by the Mo sites. Nonequivalent “up” and “down” triangles are denoted as \mathcal{T}' and \mathcal{T} , respectively.

Fermi surface that is reconstructed at low temperatures filling 2/3 of the spinon states.

However, the adequacy of the proposed mechanisms was questioned with recently synthesised $\text{Li}_2\text{InMo}_3\text{O}_8$ and $\text{Li}_2\text{ScMo}_3\text{O}_8$, both featuring magnetic moments well localised at the Mo_3O_{13} clusters. While the former was identified with a Néel 120° magnetic order at $T_N = 12$ K, for the latter no magnetic ordering has been observed down to 0.5 K [23, 24]. Instead, muon spin rotation and inelastic neutron scattering measurements suggested that $\text{Li}_2\text{ScMo}_3\text{O}_8$ undergoes a short-range magnetic order below 4 K with QSL-like excitations.

Despite having similar crystal structures, these systems manifest essentially unlike magnetic properties, whose enigmatic origin remains an unsolved problem. In this Letter, upon revising a single-orbital extended Hubbard model on the anisotropic kagomé lattice at 1/6 filling, we uncover novel regimes of the plaquette charge ordered and cluster Mott insulator states governed by the interplay of kinetic energy and intersite Coulomb interactions, that were overlooked in previous studies [21, 22, 25]. By means of first-principles calculations, we will demonstrate that their appearance is related to the formation of the Mo_3O_{13} clusters and these states indeed realise in $\text{LiZn}_2\text{Mo}_3\text{O}_8$, $\text{Li}_2\text{ScMo}_3\text{O}_8$, and $\text{Li}_2\text{InMo}_3\text{O}_8$.

The model of interest shown in Fig. 1c with one electron per \mathcal{T} triangle reads:

$$\begin{aligned} \mathcal{H} = & \sum_{\langle mm' \rangle \in \mathcal{T}} t (c_m^\dagger c_{m'}^\sigma + \text{H.c.}) + V n_m n_{m'} + U \sum_m n_m^\uparrow n_m^\downarrow \\ & + \sum_{\langle mm' \rangle \in \mathcal{T}'} t' (c_m^\dagger c_{m'}^\sigma + \text{H.c.}) + V' n_m n_{m'}, \end{aligned} \quad (1)$$

where c_m^\dagger (c_m^σ) creates (annihilates) an electron with spin σ at site m , $n_m^\sigma = c_m^\dagger c_m^\sigma$ is the density operator ($n_m = n_m^\uparrow + n_m^\downarrow$), t and t' stand for intracluster and intercluster hopping parameters defined on the \mathcal{T} and \mathcal{T}' triangles, respectively, and the interaction terms include the on-site U , intracluster V , and intercluster V' Coulomb repulsions. Taking a shorter bond length in \mathcal{T} , we assume that $V' < V \ll U$ and $|t'| < |t|$, and for the reasons shown below we enforce electron localisation at the \mathcal{T} triangles by taking $t < 0$ and $t' > 0$.

The results of exact diagonalisation for Eq. (1) at 1/6 filling are shown in Fig. 2. Specific heat has an evident instability when t/V' and t'/V are small, while as they increase the system can develop long-range magnetic order. Thus, one can see that there are several regimes depending on the values of t/V' and t'/V , and below we will address two different limits of Eq. (1).

Plaquette charge order. Let us consider $t \ll V'$ and $t' \ll V$. Due to 1/6 filling, the Hubbard U cannot localise electrons on the lattice sites, and as a result they move without encountering any double occupancy.

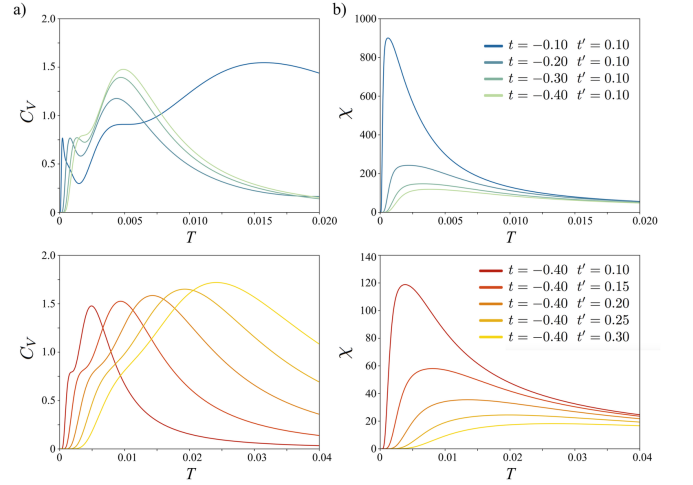


FIG. 2. Specific heat (a) and spin susceptibility (b) of the extended Hubbard model, Eq. (1), at 1/6 filling calculated with exact diagonalisation on a 2×2 supercell with 12 sites and periodic boundary conditions as a function of t and t' with $U = 2.0$, $V = 1.0$, and $V' = 0.8$.

Since U is not operative, it is the intersite V and V' that are responsible for electron localisation leading to a highly degenerate charge ordered state, where each corner-sharing triangle hosts exactly one electron. This degeneracy is further lifted by hopping parameters that induce collective tunnelling processes, when the electrons hop either clockwise or counter-clockwise along the \mathcal{T} and \mathcal{T}' bonds stabilising a charge pattern with three electrons at the hexagons, as shown in Fig. 3a and 3b. To lowest order in t/V' and t'/V , it corresponds to the quantum dimer model for two plaquette states $|\mathbb{A}\rangle = c_5^\dagger c_3^\dagger c_1^\dagger |0\rangle$ and $|\mathbb{B}\rangle = c_6^\dagger c_4^\dagger c_2^\dagger |0\rangle$,

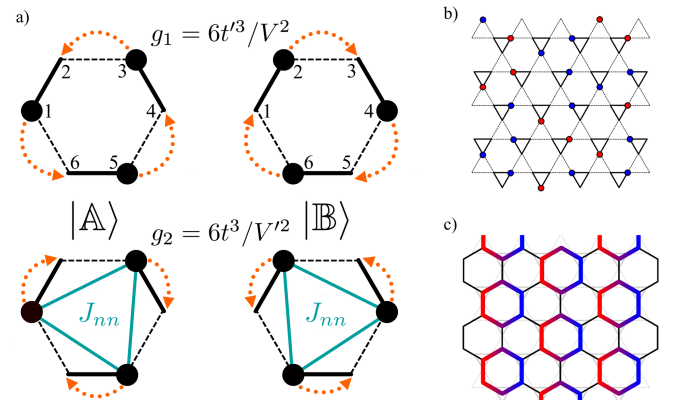


FIG. 3. a) Ring tunnelling processes in the hexagon; b) Charge order in the strong interaction limit (blue and red circles stand for the spin-up and spin-down electrons, respectively) b) Plaquette charge ordered phase on the dual hexagonal lattice.

$\mathcal{H}_\square = \sum_\square \sum_{\sigma\sigma'\sigma''} (g_1 + g_2) (|\mathbb{A}\rangle\langle\mathbb{B}| + |\mathbb{B}\rangle\langle\mathbb{A}|)$ with $g_1 = 6t^3/V^2$ and $g_2 = 6t^3/V'^2$, where the sum runs over all hexagons [29, 30]. When mapped onto the dual hexagonal lattice, the ground state of \mathcal{H}_\square for spinless electrons is described by the PCO shown in Fig. 3c with an emergent triangular lattice of resonating hexagons, that will be regarded as the strong interaction limit of Eq. (1) [31–33].

One can further include antiferromagnetic spin fluctuations between next-nearest neighbours in each hexagon $\mathcal{H}_S = J_{nn} \sum_{\langle\langle ij \rangle\rangle} n_i n_j (\mathbf{S}_i \cdot \mathbf{S}_j - \frac{1}{4})$, where $J_{nn} = 4t_{nn}^2/U$ and t_{nn} is the corresponding hopping. Assuming that the PCO effectively decouples hexagons, $\mathcal{H}_D = \mathcal{H}_\square + \mathcal{H}_S$ for a single hexagon can be solved exactly yielding four four-fold degenerate states [27]. When g_1 and g_2 have opposite signs, regardless of the value of J_{nn} the ground state of \mathcal{H}_D displays valence bond condensation with one orphan spin, as shown in Fig. 4a:

$$\begin{aligned} |\psi_1\rangle &= \frac{1}{2} \left(|\uparrow\uparrow\downarrow\rangle_{\mathbb{A}} - |\downarrow\uparrow\uparrow\rangle_{\mathbb{A}} \right. \\ &\quad \left. - \frac{g_1 - g_2}{\tilde{g}} |\uparrow\uparrow\downarrow\rangle_{\mathbb{B}} - \frac{g_2}{\tilde{g}} |\uparrow\uparrow\uparrow\rangle_{\mathbb{B}} + \frac{g_1}{\tilde{g}} |\downarrow\uparrow\uparrow\rangle_{\mathbb{B}} \right), \\ |\psi_2\rangle &= \frac{1}{2} \left(|\uparrow\downarrow\uparrow\rangle_{\mathbb{A}} - |\downarrow\uparrow\uparrow\rangle_{\mathbb{A}} \right. \\ &\quad \left. + \frac{g_2}{\tilde{g}} |\uparrow\uparrow\downarrow\rangle_{\mathbb{B}} - \frac{g_1}{\tilde{g}} |\uparrow\downarrow\uparrow\rangle_{\mathbb{B}} + \frac{g_1 - g_2}{\tilde{g}} |\downarrow\uparrow\uparrow\rangle_{\mathbb{B}} \right). \end{aligned}$$

with $\tilde{g} = \sqrt{g_1^2 - g_1 g_2 + g_2^2}$. Such an unusual entanglement with dangling spins originates solely from the asymmetry of tunnelling processes that in turn maximises singlet pairing between the resonating electrons, while the unpaired spins behave paramagnetically in a thermodynamic limit. Interestingly, a similar situation can be realised when $g_1 < 0$ and $g_2 < 0$ with large antiferro-

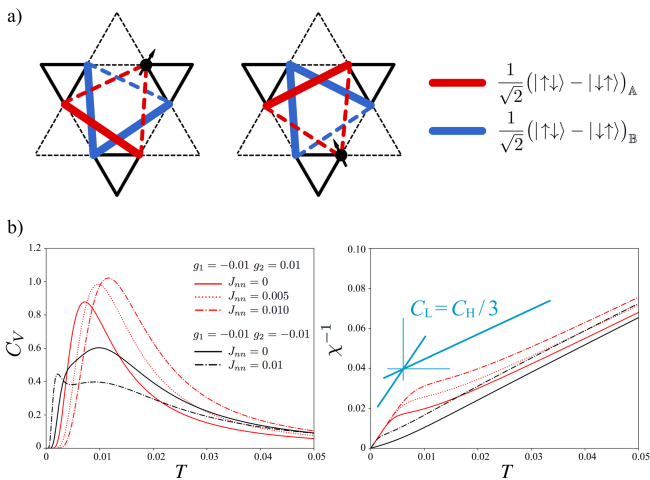


FIG. 4. a) Valence bonds at the resonating hexagon with one dangling spin; b) Specific heat and inverse spin susceptibility of a single resonating hexagon.

magnetic coupling $J_{nn} > \frac{2}{3}(-g_1 - g_2 - \tilde{g})$, which was earlier suggested to pair $2/3$ of the spins at low temperatures [22, 25]. However, the calculated thermodynamic properties shown in Fig. 4b clearly demonstrate that two paramagnetic regimes possess a much higher T_C when g_1 and g_2 have opposite signs. Our first-principles calculations will show that the strong interaction limit is realised in $\text{LiZn}_2\text{Mo}_3\text{O}_8$, where g_1 and g_2 have opposite signs and J_{nn} is negligibly small.

Cluster Hubbard Model. As $|t|$ increases, the electrons start moving freely within the \mathcal{T} triangle, and the number of electrons at the adjacent \mathcal{T}' triangles fluctuates. When $|t| \sim V'$, the perturbation theory considered above breaks down, and the electrons minimise their energy by forming bound “molecular” states. As a result, the kagomé lattice is trimerised, and the original model in Eq. (1) can be reformulated as a three-orbital extended Hubbard model on the triangular lattice formed by the \mathcal{T} triangles:

$$\mathcal{H}_{\text{CF}} = \frac{\Delta}{3} \sum_{mm' \in \mathcal{T}, \sigma} c_{im}^{\dagger\sigma} \begin{pmatrix} 0 & 1 & 1 \\ 1 & 0 & 1 \\ 1 & 1 & 0 \end{pmatrix} c_{mm'}^{\sigma}$$

with $\Delta = 3t$. As follows, \mathcal{H}_{CF} has the form of crystal field that splits the electronic states at the \mathcal{T} triangle into the single a_1 and double degenerate e_1 states with energy levels $\frac{2\Delta}{3}$ and $-\frac{\Delta}{3}$, respectively: $|a_1\rangle = \frac{1}{\sqrt{3}}(|1\rangle + |2\rangle + |3\rangle)$, $|e_1^{(1)}\rangle = \frac{1}{\sqrt{3}}(w|1\rangle + \bar{w}|2\rangle + |3\rangle)$, and $|e_1^{(2)}\rangle = \frac{1}{\sqrt{3}}(\bar{w}|1\rangle + w|2\rangle + |3\rangle)$ with $\omega = e^{2\pi i/3}$. Importantly, the a_1 state is occupied when $\Delta < 0$ ($t < 0$). Despite the weak interaction limit, the electrons are localised at the \mathcal{T} triangles by their kinetic energy due to a dilute $1/6$ filling. We refer to this state as a cluster Mott insulator as opposed to the PCO phase where localisation is entirely driven by intersite Coulomb interactions.

As shown in Fig. 2, when both $t < 0$ and $t' > 0$ are large the localised electrons can develop long-range magnetic order. In this limit, the on-site $\tilde{U} = \frac{U+2V}{3}$ comes back into play and forbids any double occupancy at the \mathcal{T} triangles, and the corresponding spin model $\mathcal{H}_\Delta = \sum_{\langle ij \rangle} J_\Delta \mathbf{S}_i \cdot \mathbf{S}_j$ on the triangular lattice can be derived to second order in t'/U and t'/Δ :

$$\begin{aligned} J_\Delta = & - \frac{8t'^2}{3(2V + 3|\Delta| - 2V')} + \frac{4t'^2}{3(U + 2V - 2V')} \\ & + \frac{8t'^2}{3(U + 2V + 3|\Delta| - 2V')}, \end{aligned} \quad (2)$$

which can be both ferro- and antiferromagnetic, that explains why some of the recently found Mo_3O_8 systems are ferromagnetic insulators [28]. Stability of the magnetic order is directly related to the strength of t and t' in the sense that it can be suppressed by thermal or quantum fluctuations when t or t' are not strong enough to avoid electron fluctuations at the \mathcal{T}' triangles.

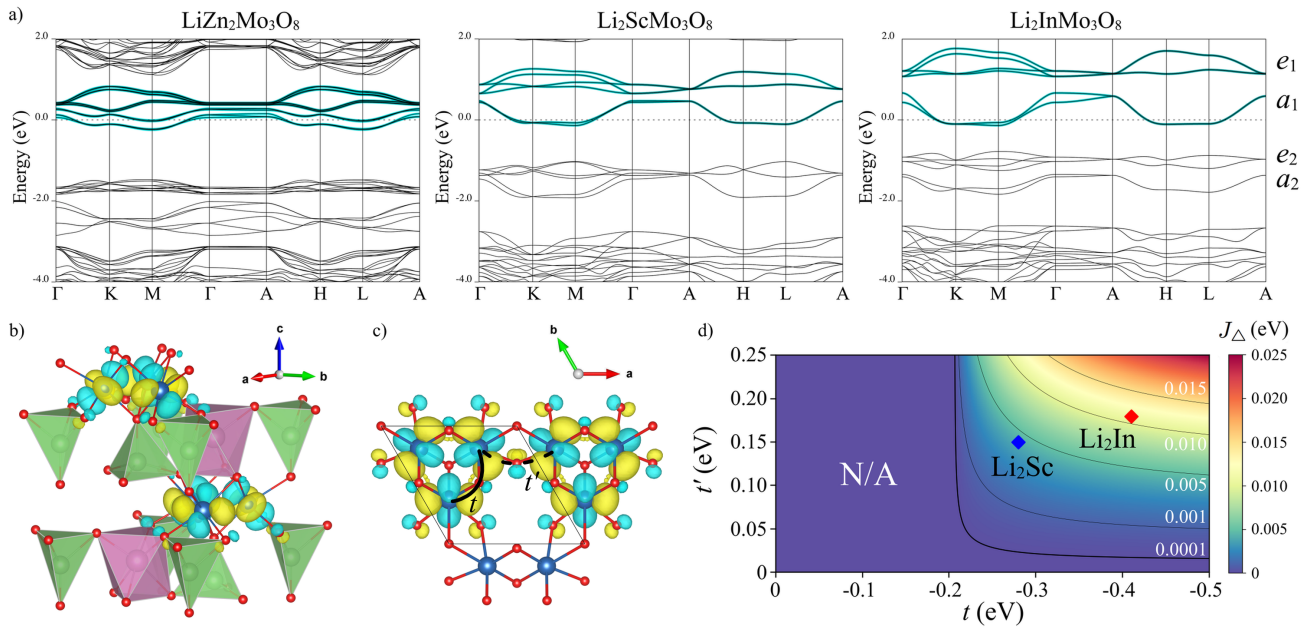


FIG. 5. a) Band structures of LiZn₂Mo₃O₈, Li₂ScMo₃O₈, and Li₂InMo₃O₈; b) Wannier functions corresponding to the a_1 and e_1 states in Li₂InMo₃O₈; c) Wannier functions of the neighbouring Mo₃O₁₃ clusters in one layer of Li₂InMo₃O₈; d) Exchange coupling J_{Δ} calculated from Eq. (2) with $U = 2.0$ eV, $V = 1.1$ eV, and $V' = 0.9$ eV. Li₂ScMo₃O₈ and Li₂InMo₃O₈ are schematically shown with diamonds.

First-principles. Electronic structure calculations for each system have been performed within local density approximation [35] by using projected augmented wave formalism [36], as implemented in VASP [37], and norm-conserving pseudopotentials, as implemented in Quantum ESPRESSO [38]. The calculated band structures are shown in Fig. 5a, indicating the a_2 and e_2 states below the Fermi level, which are responsible for the Mo-Mo bonding in the Mo₃O₁₃ cluster, and the molecular a_1 and e_1 states occupied by unpaired electrons. The latter were adopted for constructing the extended Hubbard model, Eq. (1), in the basis of Wannier functions, which were obtained with wannier90 [39], as shown in Fig. 5b. The full set of model parameters is given in Table I [27].

According to our results, the splitting between the a_1 and e_1 states varies significantly within the systems [40], and the values of t/V' and t'/V point out at different regimes of electron localisation for each system. Further-

TABLE I. Model parameters (in eV) for the one-orbital extended Hubbard model, Eq. (1).

	U	t	V	t'	V'	t_{nn}
LiZn ₂ Mo ₃ O ₈	2.0	-0.134	0.8	0.113	0.6	0.026
Li ₂ ScMo ₃ O ₈	2.0	-0.281	1.0	0.147	0.8	0.014
Li ₂ InMo ₃ O ₈	2.1	-0.409	1.2	0.181	0.9	0.010

more, t and t' always have opposite signs. This is related to the fact that in the Mo₃O₁₃ clusters with short Mo-Mo bonds the direct $d-d$ (always negative) hopping dominates, as shown in Fig. 5c. Because this term vanishes rapidly with metal-metal distance ($\sim 1/r^5$ [41]), the hopping process via common oxygens having the opposite sign starts to dominate between the clusters, and t' turns out to be positive. We believe that the opposite signs of t and t' is a fundamental aspect of the trimerised kagome lattice at 1/6 filling. According to the general Jahn-Teller theorem, the trimerisation should lift the degeneracy of the ground state so that a single electron resides at the a_1 orbital of the \mathcal{T} triangle forming a one-dimensional representation of the point group, that occurs only when $t < 0$ and $t' > 0$.

One can see that t/V' and t'/V are small in LiZn₂Mo₃O₈, preventing the electrons from being localised at the molecular states and thus leading to an emergent PCO with unpaired spins at the resonating hexagons. Moreover, a negligibly small $J_{nn} = 1.4$ meV eliminates all previously suggested scenarios for decoupling 1/3 of the spins at low temperatures [22, 25, 42]. In fact, valence bond condensation in LiZn₂Mo₃O₈ is driven solely by the asymmetry of tunnelling processes caused by the formation of the Mo₃O₁₃ clusters. Given $g_1 = 13.5$ meV and $g_2 = -40.1$ meV, the calculated $T_C \sim 92.0$ K between two paramagnetic regimes is in excellent agreement with experiments [18, 27].

In contrast, Li₂ScMo₃O₈ and Li₂InMo₃O₈ have larger

splittings between the a_1 and e_1 states, and the ratio t/V' favours electron localisation at the Mo_3O_{13} clusters stabilising a cluster Mott insulator phase. Indeed, having the largest t/V' and t'/V , $\text{Li}_2\text{InMo}_3\text{O}_8$ reveals an antiferromagnetic order with $J_\Delta = 9.5$ meV (109.8 K) in good agreement with the experimental value of 112 K [23]. On the other hand, $J_\Delta = 4.0$ meV (46.7 K) in $\text{Li}_2\text{ScMo}_3\text{O}_8$, being consistent with the experimental value of 67 K, is close to the instability region where J_Δ is small, as clearly seen in Fig. 5c. Consequently, although the electrons tend to localise at the Mo_3O_{13} clusters, $\text{Li}_2\text{ScMo}_3\text{O}_8$ is more likely to fall into an intermediate regime, where any long-range magnetic order is suppressed by quantum fluctuations down to low temperatures. Since the number of electrons at the T' triangles is allowed to fluctuate when t/V' and t'/V are not strong, we conclude that magnetic order in $\text{Li}_2\text{ScMo}_3\text{O}_8$ is short-range with QSL-like excitations.

Conclusions. Having considered an extended Hubbard model on the anisotropic kagomé lattice at 1/6 filling, we showed that it features two different limits: a plaquette charge order with one orphan spin as realised in quantum paramagnet $\text{LiZn}_2\text{Mo}_3\text{O}_8$, and a cluster Mott insulator as revealed in $\text{Li}_2\text{InMo}_3\text{O}_8$ with a Néel-type antiferromagnetic order and $\text{Li}_2\text{ScMo}_3\text{O}_8$ with a quantum spin liquid behaviour. Based on first-principles calculations, we demonstrated that their manifestation can be attributed to the trimerisation of the kagomé lattice specifying the character of electron localisation, that unravels a largely speculated origin of magnetism in these systems.

Finally, it is known that spin- $\frac{1}{2}$ systems with an odd number of electrons can reveal both long-range order and short-range correlations with topological excitations [43]. While $\text{LiZn}_2\text{Mo}_3\text{O}_8$ remains a unique example featuring two paramagnetic regimes with unpaired spins, different scenarios of a cluster Mott insulator phase can be realised in other trimerised cluster systems, such as $\text{Li}_2\text{In}_{1-x}\text{Sc}_x\text{Mo}_3\text{O}_8$ [42], $\text{ScZnMo}_3\text{O}_8$ [44], and Nb_3Cl_8 [45, 46].

Acknowledgements. S.A.N. thanks Dr. Wei Ren for stimulating discussions. I.V.S. and S.V.S. were supported by projects RFBR 20-32-70019, programs AAAA-A18-118020190095-4 (Quantum) and contract No. 02.A03.21.0006. S.V.S. is grateful for discussions to V. Irkhin, Yu. Skryabin, and D.I. Khomskii.

* nikolaev.s.aa@m.titech.ac.jp; saishi@inbox.ru

[1] R. Moessner, *Can. J. Phys.* **79**, 1283 (2001).
 [2] Patrick. A. Lee, *Science* **321**, 1306 (2008).
 [3] L. Balents, *Nature (London)* **464**, 199 (2010).
 [4] Lucile Savary, Leon Balents, *Rep. Prog. Phys.* **80**, 016502 (2017).
 [5] G. Misguich, C. Lhuillier, B. Bernu, and C. Waldtmann, *Phys. Rev. B* **60**, 1064 (1999).

[6] Olexei I. Motrunich, *Phys. Rev. B* **72**, 045105 (2005).
 [7] B. Bauer, L. Cincio, B. P. Keller, M. Dolfi, G. Vidal, S. Trebst, and A. W. W. Ludwig, *Nat. Commun.* **5**, 5137 (2014).
 [8] Shou-Shu Gong, Wei Zhu, and D. N. Sheng, *Scientific reports* **4**, 6317 (2014).
 [9] Yi Zhou, Kazushi Kanoda, Tai-Kai Ng, *Rev. Mod. Phys.* **89**, 025003 (2017).
 [10] Z. Hiroi, M. Hanawa, N. Kobayashi, M. Nohara, and H. Takagi, *J. Phys. Soc. Jpn.* **70**, 3377 (2001).
 [11] J. S. Helton *et al.*, *Phys. Rev. Lett.* **98**, 107204 (2007).
 [12] A. Olariu, P. Mendels, F. Bert, F. Duc, J. C. Trombe, M. A. de Vries, and A. Harrison, *Phys. Rev. Lett.* **100**, 087202 (2008).
 [13] Y. Shimizu, K. Miyagawa, K. Kanoda, M. Maesato, and G. Saito, *Phys. Rev. Lett.* **91**, 107001 (2003).
 [14] T. Itou, A. Oyamada, S. Maegawa, M. Tamura, R. Kato, *J. Phys. Conf. Ser.* **145**, 012039 (2009).
 [15] T. Itou, A. Oyamada, S. Maegawa, M. Tamura, R. Kato, *Phys. Rev. B* **77**, 104413 (2008).
 [16] W. H. McCarrroll, *Inorg. Chem.* **16**, 3351 (1977).
 [17] F. A. Cotton, *Inorg. Chem.* **3**, 1217 (1964).
 [18] J. P. Sheckelton, J. R. Neilson, D. G. Soltan and T. M. McQueen, *Nat. Mater.* **11**, 493 (2012).
 [19] M. Mourigal, W. T. Fuhrman, J. P. Sheckelton, A. Wartelle, J. A. Rodriguez-Rivera, D. L. Abernathy, T. M. McQueen, and C. L. Broholm, *Phys. Rev. Lett.* **112**, 027202 (2014).
 [20] J. P. Sheckelton *et al.*, *Phys. Rev. B* **89**, 064407 (2014).
 [21] Rebecca Flint and Patrick A. Lee, *Phys. Rev. Lett.* **111**, 217201 (2013).
 [22] Gang Chen, Hae-Young Kee, and Yong Baek Kim, *Phys. Rev. B* **93**, 245134 (2016).
 [23] Yuya Haraguchi, Chishiro Michioka, Masaki Imai, Hiroaki Ueda, and Kazuyoshi Yoshimura, *Phys. Rev. B* **92**, 014409 (2015).
 [24] Kazuki Iida *et al.*, *Sci. Rep.* **9**, 1826 (2019).
 [25] Gang Chen and Patrick A. Lee, *Phys. Rev. B* **97**, 035124 (2018).
 [26] K. Momma and F. Izumi, *J. Appl. Crystallogr.* **44**, 1272 (2011).
 [27] See Supplemental Material at [] for the full set of model parameters and calculation details, which includes Refs. [47–51].
 [28] R. P. Sinclair, PhD Thesis, University of Tennessee, 2018.
 [29] R. Moessner, S. L. Sondhi, and P. Chandra, *Phys. Rev. B* **64**, 144416 (2001).
 [30] Thiago M. Schlittler, Rémy Mosseri, and Thomas Barthel, *Phys. Rev. B* **96** 195142 (2017).
 [31] F. Pollmann, P. Fulde, and K. Shtengel, *Phys. Rev. Lett.* **100**, 136404 (2008).
 [32] Satoshi Nishimoto, Masaaki Nakamura, Aroon O'Brien, and Peter Fulde, *Phys. Rev. Lett.* **104**, 196401 (2010).
 [33] A. O'Brien, F. Pollmann, P. Fulde, *Phys. Rev. B* **81**, 235115 (2010).
 [34] Here, $|\psi_3\rangle$ and $|\psi_4\rangle$ are obtained by applying time-reversal symmetry to the above states.
 [35] W. Kohn, L. J. Sham, *Phys. Rev. A* **140**, 1133 (1965).
 [36] P. E. Blochl, *Phys. Rev. B* **50**, 17953 (1994).
 [37] G. Kresse, J. Hafner, *Phys. Rev. B* **47**, 558 (1993).
 [38] P. Giannozzi *et al.*, *J. Phys.: Condens.Matter* **21**, 395502 (2009).
 [39] A. A. Mostofi, J. R. Yates, G. Pizzi, Y. S. Lee, I. Souza, D. Vanderbilt, N. Marzari, *Comput. Phys. Commun.*

- 185**, 2309 (2014).
- [40] In $\text{LiZn}_2\text{Mo}_3\text{O}_8$, there is a small splitting between the a_1 and e_1 states corresponding to different Mo layers due to disorder of Li and Zn ions.
- [41] W. A. Harrison, *Elementary Electronic Structure* (World Scientific, Singapore, 1999).
- [42] A. Akbari-Sharbat, R. Sinclair, A. Verrier, D. Ziat, H. D. Zhou, X. F. Sun, and J. A. Quilliam, *Phys. Rev. Lett.* **120**, 227201 (2018).
- [43] M. B. Hastings, *Phys. Rev. B* **69**, 104431 (2004).
- [44] C. C. Torardi, R. E. McCarley, *Inorg. Chem.* ,**24**, 476 (1985).
- [45] Yuya Haraguchi, Chishiro Michioka, Manabu Ishikawa, Yoshiaki Nakano, Hideki Yamochi, Hiroaki Ueda, Kazuyoshi Yoshimura, *Inorg. Chem.* 56, 3483 (2017).
- [46] J. P. Sheckelton, K. W. Plumb, B. A. Trump, C. L. Broholm, and T. M. McQueen, *Inorg. Chem. Front.* **4**, 481 (2017).
- [47] H. J. Monkhorst, J. D. Pack, *Phys. Rev. B* 13, **5188** (1976).
- [48] N. Marzari, A. A. Mostofi, J. R. Yates, I. Souza, and D. Vanderbilt, *Rev. Mod. Phys.* **84**, 1419 (2012).
- [49] M. Springer and F. Aryasetiawan, *Phys. Rev. B* **57**, 4364 (1998).
- [50] F. Aryasetiawan, M. Imada, A. Georges, G. Kotliar, S. Biermann, and A. I. Lichtenstein, *Phys. Rev. B* **70**, 195104 (2004).
- [51] Frank Pollmann, Krishanu Roychowdhury, Chisa Hotta, and Karlo Penc, *Phys. Rev. B* **90**, 035118 (2014).